THz-TDS time trace analysis for physical parameters extraction

Romain Peretti, Sergey Mitryukovskiy, Kevin Froberger, Aniss Merbarki, Sophie Eliet Eliet-Barois, Mathias Vanwolleghem, Jean-Francois Lampin

THz-TDS time trace analysis for physical parameters extraction

Romain Peretti, Sergey Mitryukovskiy, Kevin Froberger, Aniss Merbarki, Sophie Eliet, Mathias Vanwolleghem, Jean-François Lampin

***Abstract*—We report on a method and an associated open source software, Fit@TDS, working on an average personal computer. The method is based on the fitting of a time-trace data of a terahertz time-domain-spectroscopy system enabling the retrieval of the refractive index of a dielectric sample and the resonance parameters of a metasurface (quality factor, absorption losses, etc.). The software includes commonly used methods where the refractive index is extracted from frequency domain data. However, these methods are limited, for instance in case of a high noise level or when an absorption peak saturates the absorption spectrum bringing the signal to the noise level. Our software allows to use a new method where the refractive indices are directly fitted from the time-trace. The idea is to model a material or a metamaterial through parametric physical models (Drude-Lorentz model and time-domain coupled mode theory) and to implement the subsequent refractive index in the propagation model to simulate the time-trace. Then, an optimization algorithm is used to retrieve the parameters of the model corresponding to the studied material/metamaterial. In this paper, we explain the method and test it on fictitious samples to probe the feasibility and reliability of the proposed model. Finally, we used Fit@TDS on real samples of high resistivity silicon, lactose and gold metasurface on quartz to show the capacity of our method**

***Keywords:* Electromagnetic modeling, Refractive index, spectroscopy, Terahertz materials, Terahertz metamaterials.**

I. Introduction

THE method of teraHertz time-domain spectroscopy (THz-TDS) enabled by the progress of short pulses lasers, has begun to develop rapidly about 30 years ago [1, 2, 3, 4].This technic is now mature and set-ups are commercialized by several companies. Today, THz-TDS is the main tool for broadband terahertz (THz) spectroscopy, offering more than one-decade bandwidth with a standard resolution up to ~ 1 GHz. THz-TDS has shown the capability to study different materials such as semiconductors [5], ferroelectrics, superconductors, liquids [6], gases [7, 8], biomolecules [9] molecular crystal such as carbohydrates [10]. More recently, the measurements of band-pass filters [11] and metasurfaces embedded in microfluidic circuitry [12] were presented along with more fundamental studies of, for instance, ultra-strong coupling [13, 14].

The basic specificity of this spectroscopic technic reads in its name: measurements are not done in the frequency domain using a dispersive element, but in the time domain. In addition, in contrast to Fourier transform infrared spectrometer, in which the measured function is the self-correlation of the time data through interferometry, THz-TDS is based on a direct measurement of the electric field versus time in the THz frequency range.

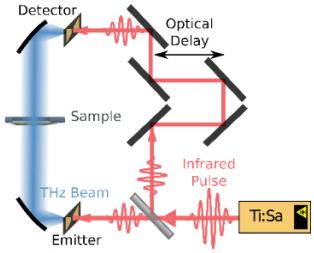

FIG. 1. Schematic of a typical THz-TDS experiment. It shows the femtosecond Ti:Sa laser exciting a photoconductive antenna that produces a THz pulse. This pulse travels through the sample and is then detected by another photoconductive antenna when illuminated with the femtosecond laser pulse after a controlled delay.

The working principle of a common THz-TDS setup is depicted in FIG. 1. A THz pulse is emitted by a THz antenna or a nonlinear crystal by means of optical rectification effect of a near infrared pulse produced by a femtosecond laser.

"This work was partially supported by: i) the international chair of excellence "ThOTroV" from region "Hauts-de-France" ii) the welcome talent grant NeFiStoV from European metropole of Lille and iii) the French government through the National Research Agency (ANR) under program PIA EQUIPEX ExCELSiOR ANR 11-EQPX-0015."

All Authors are with the Institut d'Electronique de Microélectronique et de Nanotechnologie (IEMN), CNRS, Univ. Lille, 59652 Villeneuve d'Ascq, France (corresponding author: romain.peretti@univ-lille.fr).

Next, a lens or a parabolic mirror is used to collimate the pulse and to direct it towards the studied sample. The transmitted (or reflected) pulse is then collected by an optical system to a detector. The detector measures the electric field versus time by means of photoconductive or electro-optical sampling with a typical time sampling between 10 and 50 fs.

The ability to measure directly the electric field of the THz pulse rather than the averaged energy gives access to both the phase and the amplitude of the waveform, and thus provides the information on the absorption coefficient and the refractive index of the sample, or on the dispersion [15] in case of a photonic element like a waveguide. This makes the THz-TDS method a powerful tool for characterization of materials and photonic devices. For material analysis, the usual way to retrieve material parameters is to perform a Fourier transform of the recorded pulse time-traces with and without a sample (respectively $E_s(t)$ and $E_{ref}(t)$ are the time signals, and $\tilde{E}_s(\omega)$ and $\tilde{E}_{ref}(\omega)$ are their Fourier transforms[1]) the ratio between these two spectra is called the complex transmission coefficient and writes [16, 17]:

$$\tilde{T}(\omega) = \frac{\tilde{E}_s(\omega)}{\tilde{E}_{ref}(\omega)}$$

$$\tilde{T}(\omega) = \tilde{s}(\omega) \times exp\left(-j\frac{\omega d}{c}(\tilde{n}(\omega) - 1)\right) \times \widetilde{FP}(\omega)\,, \tag{1}$$

here $\tilde{n}$ is the complex refractive index where the real part corresponds to a delay and the imaginary part - to an absorption in the material, *d* is the thickness of the sample that has to be measured, and *ω* is the angular frequency. The term $\tilde{s}(\omega)$ is the product of the Fresnel coefficients at normal incidence for the two air/material interfaces:

$$\tilde{s}(\omega) = \tilde{t}_{1\to2}(\omega) \times \tilde{t}_{2\to1}(\omega) = \frac{4\tilde{n}(\omega)}{(\tilde{n}(\omega)+1)^2}\,. \tag{2}$$

Finally, $\widetilde{FP}(\omega)$ is a term taking into account the Fabry-Pérot multiple reflections in the sample [18]:

$$\widetilde{FP}(\omega) = \frac{1}{1 - \left(\tilde{r}_{2\to1}(\omega)\right)^2 exp\left(-2j\frac{\omega d}{c}\tilde{n}(\omega)\right)}\,. \tag{3}$$

The formula (1) sets the so-called “forward problem”: knowing $\tilde{E}_{ref}(\omega)$ and $\tilde{n}(\omega)$ one can get $\tilde{E}_s(\omega)$. Since the experiment gives $\tilde{E}_{ref}(\omega)$and $\tilde{E}_s(\omega)$ the actual interest is the “inverse problem”. It means that knowing $\tilde{E}_{ref}(\omega)$ and$\tilde{E}_s(\omega)$, one can get$\tilde{n}(\omega) = \tilde{\eta}(\omega) + \tilde{\kappa}(\omega)$. As far as our knowledge, this problem can be analytically solved only ignoring the Fabry-Pérot term (for example using a temporal filtering) and only for a sample without absorption. Since these hypotheses imply that there is no phase term in the transmission (2), the method consists in the extraction of the unwrapped phase from the THz-TDS data in the frequency domain and then in its division by the frequency to get the refractive index. Additionally, since another implication from those hypotheses is that there is no losses during the pulse propagation, one can retrieve the transmission versus frequency and solve the second order equation from (2) to retrieve the refractive index. Consequently, this method excludes most of the samples (optically thin samples *nd* < 1.5 mm, and absorbing samples, for instance) and is thus very limited. Nevertheless, one can iterate this process by getting the real part of the refractive index from the unwrapped phase and then compensate the difference of the losses by adding an imaginary term to the refractive index. Then, one has to compensate the phase term in the transmission due to this imaginary part and thus come back to the beginning of the loop. This iterative method is a good starting point; however, it does not guaranty the convergence or any reliability of the obtained results since you do not respect causality anymore, there is a room for improvement by solving this inverse problem with a numerical approach. To do so, one should define an error function, which has to be minimized. This error function could be defined as [4]:

$$\xi\big(\tilde{n}(\omega)\big)(\omega) = \big(\delta\rho(\omega)\big)^2 + \psi\big(\delta\varphi(\omega)\big)^2, \tag{4}$$

where ***δρ*** is the modulus error and ***δφ*** is the phase error between the modeled transmission coefficient $\tilde{T}$ and the measured one $\tilde{T}_{meas}$. *Ψ* is a weighting coefficient enabling the addition of the phase and modulus errors, its value is usually set to 1 *amplitude unit/rad*. The error function is defined for each frequency. Since the refractive index is related to the phase, a special attention has to be taken while calculating ***δφ***. The measured phase is calculated as the unwrapped phase of $\tilde{T}_{meas}$ and the modeled phase is calculated as following:

[1] We took as a convention that all temporal functions are denoted with a letter and their Fourier transform with the same letter and a tilde.

$$\arg\left(\tilde{T}(\omega)\right) = \arg\left(\frac{4\tilde{n}(\omega)}{(\tilde{n}(\omega)+1)^2}\right) - \frac{\omega d}{c}(\tilde{n}(\omega)-1) + \arg\left(\widetilde{FP}(\omega)\right) . \quad (5)$$

Once the error function is defined, a minimization algorithm has to be used. For example, on can use the simplex method (gradient free method) [19] or a quasi-Newton algorithm [20, 21]. The parameter research has to be done for every single frequency and gives as a result the real and the imaginary parts of the refractive index: $\tilde{\eta}(\omega)$ and $\tilde{\kappa}(\omega)$, respectively.

The method is fast and works with or without taking into account the Fabry-Pérot effect. However, the result does not respect causality (which takes the form of the Kramers-Kroenig relations in this problem) and has a big issue during the unwrapping step. Indeed, it strongly depends on the signal to noise ratio. It has been showed that it is possible to partially solve this problem by including a correction to the unwrapped measured phase using partial Kramers-Kronig relations [22]. Moreover, in the error function (4) both the modulus and the phase errors have the same weight, this is arbitrary and any choice of weighting other than 1 *amplitude unit/rad* could improve or diminish efficiency and accuracy of the algorithm.

Both the iterative and the optimization technics show good results, but are still limited: one will need the precise measurement of the thickness or the implementation of an additional optimization step [23]. In addition, a low signal to noise ratio of the measured data or a strong absorption in the sample lead to difficulties in getting the refractive index following the Kramers-Kroenig relations since the phase is lost in the frequency range where the signal value is below the noise level [22]. It implies an additional step while performing the phase unwrapping. This phase includes additional assumptions in the number and in shape of the absorption peaks. In addition, the arbitrary weighting between the phase and the amplitude, as well as an arbitrary limitation of the bandwidth to avoid the range of low signal to noise ratio, limits the robustness and thus the spreading of the optimization method.

Nevertheless, with the refractive indices retrieved by those technics, it is possible to extract further information about the material itself. For this purpose, the refractive indices are fit using models such as the Drude-Lorentz one [18, 24]. One then could get the insight of the physical properties of the studied material, such as electronic or vibrational resonances. Knowledge of these parameters is of the prime importance for the material identification; this is, for instance, one of the most promising THz applications for drug component quality control or anti-counterfeiting measure. Most approaches focus on the intensity and the resonance frequencies while some take into account the linewidth [24]. Such parameter retrievals were achieved for instance thanks to an optimization algorithm [25, 26] such as genetic algorithms [27] used in the frequency domain. Generally, the principle steps are the following: *(i)* performing the experiments with and without samples; *(ii)* performing the Fourier transform; *(iii)* measuring the thickness of the sample; *(iv)* getting the real part and/or imaginary part of the refractive index and *(v)* fitting the refractive index to get the material parameters. This process has shown good results, however, it has several drawbacks. First, such methods are intrinsically limited by the precision achieved in the measurements of the sample thickness. Second, it does not respect the causality since the equation does not respect the Kramers-Kroenig equation as the imaginary and the real parts of the refractive index are split [22]. Third, a problem arises when a sample absorbs too much so the signal value is actually going below the noise level in the frequency domain. Finally, such process is long and tedious.

In this paper, we present a robust and generic optimization approach. The software called Fit@TDS is based on the direct comparison of the initial time-domain data of the measured THz pulse with the modeled one's. We introduce a software based on the described method, allowing the modelling of simple materials, as silicon; as well as more complex ones, such as carbohydrates; and even metasurfaces.

The paper is organized as follows. The basics of the implemented optimization is explained in section II. The two different models used are quickly described in section III. The section IV consists the analysis of the methods performances on fictitious samples section V on real samples.

II. Optimization problem

The optimization problem is a problem of finding the best solution from all the feasible solutions. In the studied case, it starts with two items:

1. A set of data containing the time traces with and without a sample (2 traces);
2. A model depending on the set of parameters $\{p_i\}$ depicting how the sample transforms the reference pulse into the modeled one $E_{model}\{p_i\}(t)$.

Concretely, an example of a model for a doped semiconductor sample measured in transmission would transform $E_{ref}(t)$ to $E_{model}\{p_i\}(t)$ simply by convoluting $\tilde{E}_{ref}(\omega)$ by $T\{p_i\}(t)$ calculated by introducing the Drude-Lorentz model equation in the refractive index in (1) (see part III for details).

Then, the objective function to minimize will be set as the L^2 norm (square root of the sum of the square of the differences) of the difference between the modeled pulse and the measured (sample) one:

$$Obj\{p_i\} = \sum_{t=0}^{t=t_{max}} \left(E_{model}\{p_i\}(t) - E_s(t)\right)^2 dt\,. \tag{6}$$

This function will vary upon the value of parameters of the chosen model and the goal of the optimization is to determine the set of parameters that minimizes the objective function. An important remark here is that the function we are minimizing is proportional to electromagnetic energy. The fact that the L^2 residual error is an understandable physical quantity will help the user in interpreting the results to understand any discrepancy or mistake in both the experiment and the model. This will, for instance, facilitate the understanding of any divergence or convergence of the fit algorithm to some local minimum, or even the finding of a mistake in the choice of the model during the optimization.

The other practical advantage of this formulation is given by the Parseval theorem stating that the norm of a function is the same as the norm of its Fourier transform, meaning:

$$Obj\{p_i\} = \sum_{\omega=-\omega_{min}}^{\omega=-\omega_{max}} \left|\tilde{E}_{model}\{p_i\}(\omega) - \tilde{E}_s(\omega)\right|^2 d\omega\,. \tag{7}$$

This is extremely convenient, allowing the calculation of the objective function in both time and frequency domains without performing a Fourier transform at each iteration. Specifically, since, to our knowledge, all the refractive index models are defined in the frequency domain, this formula allows the performance of the time-domain optimization while computing the objective function in the frequency domain.

To perform the optimization we coded the methods as given in repository from ref [28] in a mainstream language Python that allows the use of different optimization libraries. Since our goal is to offer to the community a broad tool usable regardless of the type of the studied sample and subsequent problem to solve, we implement an algorithm from a research library [29] including many different algorithms giving a user an opportunity to pick the best one for its samples. For the choice of the algorithm itself, we pick a versatile one called ALPSO - Augmented Lagrangian Particle Swarm Optimizer [30]. This algorithm is an improvement to the basic “swarm particle optimization” approach regarding constrained engineering design of the optimization problem.

III. Models

We implemented two different models: one for solid materials and one for metamaterials. In both cases, we assume that the sample is only made of one layer meaning two interfaces added to a propagating medium.

A. Multiple Drude-Lorentz Model

Bulk solid materials play a role in the pulse propagation simply due to their refractive index in equation (1) and in the Fabry-Pérot term therein. Since it is the most used for solid samples, we implemented the Drude-Lorentz model that defines the dielectric permittivity of a sample as a set of electronic resonators (matrix vibrations, oscillating charges, etc) leading to the permittivity function written as:

$$\tilde{\varepsilon}(\omega) = \tilde{n}^2(\omega) = \varepsilon_\infty + \frac{\omega_p^2}{\omega^2 + j\omega\gamma_p} + \sum_{k=1}^{k_{max}} \frac{\Delta\varepsilon_k \omega_{0,k}^2}{\omega_{0,k}^2 - \omega^2 + j\omega\gamma_k}\,, \tag{8}$$

where ε_∞ is the dielectric permittivity at high frequency compared to the range of interest, ω_p is the plasma frequency, γ_p is the damping rate, k_{max} is the number of considered oscillators, ω_{0k} , γ_k and $\Delta\varepsilon_k$ are the resonant frequency, the damping rate and the strength (expressed in permittivity units) of the kth oscillator, respectively. This formula will be useful to model the phonon line in a semiconductor or in a molecular crystal in the THz range.

To summarize, in the case of a single uniform layer, the propagation will be modeled through the Fresnel coefficients and the multiple Drude-Lorentz oscillator model using $3 \times [k+1]$ parameters.

B. Metasurface

For a metamaterial, the model is different. Indeed, one has to take into account the refractive index of the material used to build the metamaterial, and in addition, the interaction of the THz pulse with the metamaterial structure itself. For resonating metasurface, one can use the time-domain coupled-mode theory (tdcmt) [31]. This theory describes how the light interacts with a photonic resonator. This approach has been used, for instance, to model an integrated photonic resonator [31] or, in the free space case (which is closer to the scope of our paper), a photonic crystal in a solar cell [32]. Thus, it is fully appropriate for a metasurface build out of resonators such as the split ring resonators. We derived a similar equation as in [31] adding the reflection and the transmission at the Air/sample interfaces and the result gives:

$$\begin{aligned}\tilde{r}_{\text{meta}}(\omega) &= \frac{S_{-1}(\omega)}{S_{+1}(\omega)} \\ &= \tilde{r}_{2\to1}(\omega) - \frac{exp(j\delta\theta)}{\sqrt{\tau_{e2}\tau_{e1}}\left(j(\omega-\omega_0)+\frac{1}{\tau_0}+\frac{1}{\tau_e}\right)}, \\ \tilde{t}_{\text{meta}}(\omega) &= \frac{S_{-2}(\omega)}{S_{+1}(\omega)} \\ &= \tilde{t}_{1\to2}(\omega) - \frac{1}{\tau_{e1}\left(j(\omega-\omega_0)+\frac{1}{\tau_0}+\frac{1}{\tau_e}\right)},\end{aligned} \tag{9}$$

where $\tilde{r}_{2\to1}(\omega)$ and $\tilde{t}_{1\to2}(\omega)$ are the reflection and the transmission coefficients shown in FIG. 2. following the Fresnel law. τ_0 is absorption losses characteristic time, τ_e, τ_{e1} and τ_{e2} the external losses characteristic time respectively total, toward direction 1 (incoming) and 2 (outgoing); ω_0 the resonant frequency of the mode.

Note that an additional hypothesis arises here: we assume that the metal of the metasurface does not influence the transmission or reflection outside from the resonance spectral ranges, meaning that the filling factor (area ratio) of the metal has to be very low.

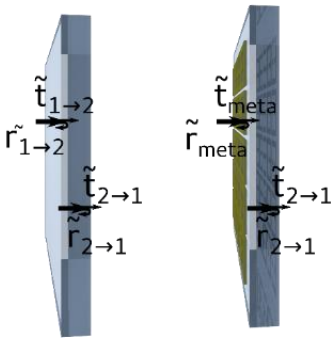

FIG. 2 Schematic showing the Fresnel coefficients for the simple layer A & the metasurface B as in equation (9).

Equation (9) will play a role in changing the transmission term:

$$\tilde{s}(\omega) = \tilde{t}_{\text{meta}}(\omega) \times \tilde{t}_{2\to1}(\omega) = \tilde{t}_{\text{meta}}(\omega)\frac{2\tilde{n}(\omega)}{(\tilde{n}(\omega)+1)}, \tag{10}$$

and in the Fabry-Pérot term that will be then written as:

$$\widetilde{FP}(\omega) = \frac{1}{1-\tilde{r}_{\text{meta}}(\omega)\tilde{r}_{2\to1}(\omega)exp\left(-2j\frac{\omega d}{c}\tilde{n}(\omega)\right)}. \tag{11}$$

To summarize, in the case of a metasurface, the substrate will again be modelled using the same Drude-Lorentz parameters with 5 additional parameters to take into account the resonant nature of the transmission and the reflection at the metasurface interfaces (frequency internal and external losses).

C. Implementation

The proposed models involve from four to more than thirty parameters for complex samples, thus the exhaustive error calculation to reach the global maximum for each set of parameters is too demanding. As stated above, the strategy we use is to implement an optimization algorithm to solve this nonlinear problem. Tremendous amount of algorithms have been developed giving birth to several fields of research. We implemented a library offering several algorithms: the optimization package called PyOpt [29]: “PyOpt is a Python-based package for formulating and solving nonlinear constrained optimization problems”. The main advantages of this package is that it includes 20 different optimization algorithms allowing the future expert users of Fit@TDS to change the algorithm for one that is more efficient in the case of his specific problem. In addition, PyOpt allows the parallelization, which is extremely useful to diminish the computation time. Since the problem is to find a global maximum rather than a local one we choose the Augmented Lagrangian Particle Swarm Optimizer (ALPSO) among the proposed algorithms. The particle swarm algorithm is a metaheuristic method meaning it makes no or few assumptions about the problem being optimized and can search very large spaces of candidate solutions [33, 34]. In other words, it is a very versatile method to solve an optimization problem. The ALPSO is an optimized version of such an algorithm. The drawback of this versatile choice is that it is not optimized to be fast for our(s) specific problem(s) and therefore, a perspective of this work will be to design or implement an algorithm more specific to this/these problem(s).

IV. Validation and Performance Assessment with Simulated Factitious Samples

To validate and assess the performances of the proposed methods we first used a simulated sample. To do so we recorded the reference spectrum with the TeraSmart THz-TDS spectrometer by Menlo Systems GmbH (1000 accumulations) [35] and then numerically simulated the response of the system with a sample using the equations described above. The data without a sample were windowed at the end of the time trace on a segment length corresponding to the time delay introduced by the sample to remove folding effect due to the periodicity of the FFT. For the data with the simulated sample, we convoluted the measured pulse by the transfer function of equation (1) with the Drude-Lorentz model inside to define the permittivity. Then, we added to the time trace a Gaussian white noise at a magnitude equivalent to the level of the high frequency noise one can observe in FIG. 3 (amplitude being 5.10^{-5} of the unit used ~ - 90 dB compared to maximum power spectral density). We used these two time traces data as the input of the Fit@TDS.

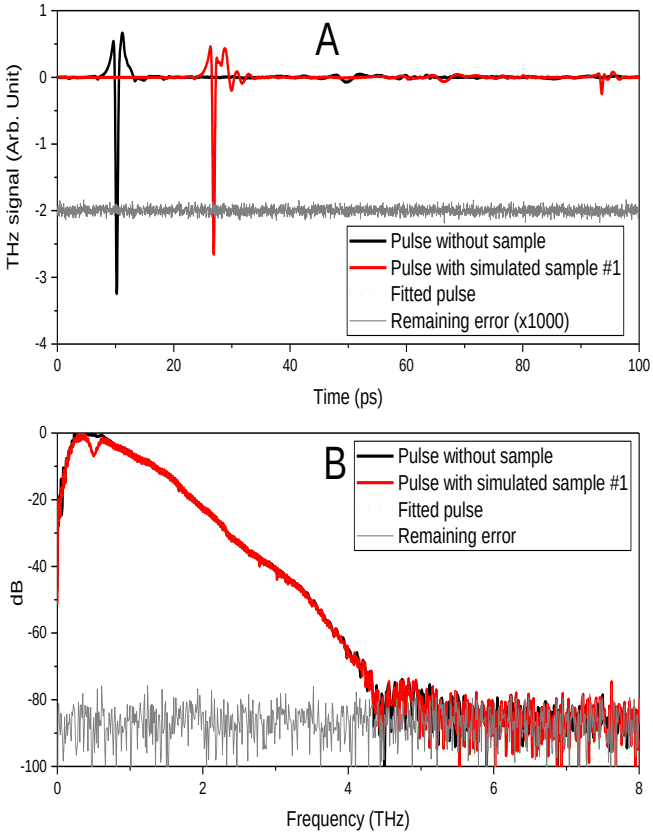

FIG. 3 (A) Time traces recorded in the THz-TDS experiments: in black – the reference, in red – simulated time trace from one oscillator sample, in green - result of the fit, in gray - the difference between the fit and the simulated data (multiplied by one thousand; (B) corresponding spectra.

A. First validation: one oscillator Drude-Lorentz model

To perform a first validation we tested Fit@TDS with a simulated 5-mm-thick sample with a dielectric constant build with the one-oscillator Drude-Lorentz model with the following parameters: $\varepsilon_\infty = 4$; $\Delta\varepsilon = 0.01$; $\omega_0 = 0.5THZ$; $\gamma = 0.1Thz$. The time race of the sample is given - in FIG. 3 the resulting permittivity is plotted in FIG. 4.

The spectral data clearly expresses a deep at the frequency of the oscillator. Then, we used our software Fit@TDS with the ALPSO algorithm using the swarm-size of 1 000, 6 inner iterations and 20 outer iterations. The bounds for the thickness were ±1 % around 5 mm. The bounds for the four other parameters were – 50% and +100% of the parameter. Although we did not optimize neither the choice of the algorithm or the parameters (swarm size, inner and outer iterations …), it took about 1 minute on a common personal computer (Intel® Core™ i7-5600U CPU @ 2.60 GHz) to retrieve the parameters from a 300 points long data. Indeed it strongly depends on the size (volume) of the space where the parameters vary and thus on the bounds we gave. On FIG. 3 on the difference, one can see extremely small discrepancy between the targeted time trace and the fitted one corresponding to the added noise. Here it is clear that the discrepancy comes from the noise added to the simulated sample time trace meaning that the algorithm was converged and that the L^2 residual error is simply the L^2 of the added noise. The results for the Drude-Lorentz parameters are very close to the targeted ones, the relative error is $E(\varepsilon_\infty) = 10^{-7}$; $E(\Delta\varepsilon) = 6.10^{-5}$; $E(\omega_0) = 8.10^{-6}$; $E(\gamma) = 8.10^{-5}$ and $1.10^{-7}$for the thickness discrepancy.

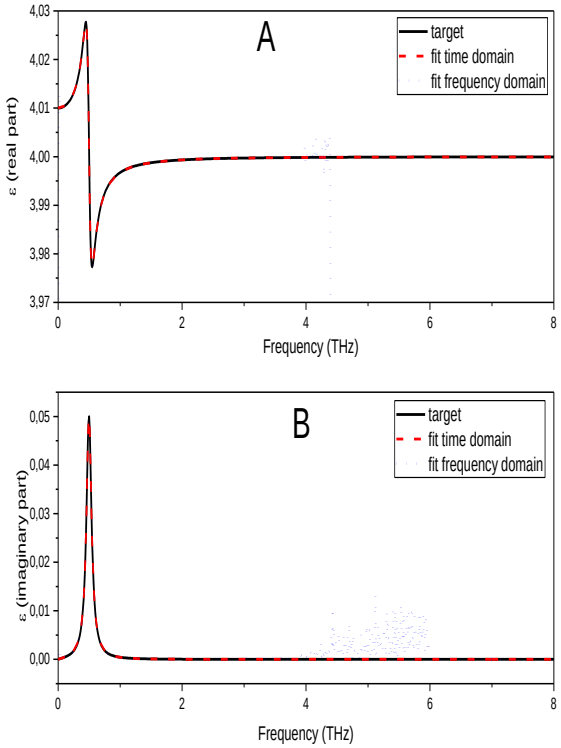

FIG. 4 Simulated and fitted electromagnetic permittivity: (A) real part, (B) imaginary part.

The error of the thickness should be compared to the delay line uncertainty:

$$\delta d = \frac{c\delta t}{\eta} \sim 9\ 10^{-7} m. \tag{12}$$

The errors on ε and $\Delta\varepsilon$ are to be compared to:

$$\delta\varepsilon = 2\left(\frac{c\delta t}{d}\right)\sqrt{\varepsilon} \sim 7\ 10^{-4}, \tag{13}$$

Which correspond to the time sampling of our THz-TDS setup. The errors on ω_0 and γ are to be compared to the frequency sampling:

$$\delta\omega = \frac{2\pi}{\Delta T} \sim 6\ 10^{10} rad/s \tag{14}$$

All results show that for a Lorentz modeled, not noisy limited time trace (see eq 15), the proposed methods and the software are validated and reach the goals without any restrictions.

B. Dependency of the error on the signal to noise ratio

To evaluate better the real life performance of the method we tested its robustness by increasing the amount of noise added to both time traces with and without a sample. Concretely, the amplitude of the Gaussian white noise was increased from 5.10^{-5} up to 5.10^{0} amplitude unit giving a dynamics from 105 dB down to 5 dB. Then, the algorithm was used to find back the parameters using the same bounds as in the previous case. The relative error of the parameters in function of the signal dynamics are given in FIG. 5. The L^2 residual error was not plotted because it always correspond to the added noise here plotted as the noise floor.

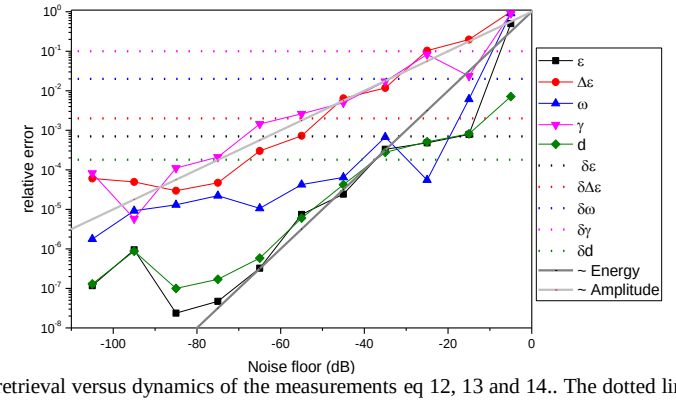

FIG. 5. Relative error on the parameters retrieval versus dynamics of the measurements eq 12, 13 and 14.. The dotted lines depicts the usual comparison point in term of precision.

Firstly, one can see that, as expected, globally the errors increase with the increase of the noise. Secondly, the relative error follows a trend between proportional to the amplitude and proportional to the energy. Thirdly, the relative uncertainty is bigger for γ and $\Delta\varepsilon$ simply because those parameters are smaller by essence. Finally, one can compare the retrieval precision with the value mentioned above and plotted in dotted lines on the same figure: it is clear that when the noise is low we (over)reach the expected precision for each parameter. Furthermore, we reach a precision bellow one percent for a noise floor of - 40 dB. This value of noise is in fact the “single shot” one in our experiments (meaning one scan by the THz-TDS delay line taking ~ 20 ms of acquisition time). This result means that the method is robust enough to allow the following of the parameters of the one-oscillator Drude-Lorentz model accurately at a noise level corresponding to the one when performing the experiments at 20 Hz repetition (video frame time). This will allow for instance to follow the temporal evolution of a chemical physical parameter extracted from the model (typically the width of an oscillator may depend on temperature) at this time frame.

C. *Resolution test*

The previous results show a very accurate retrieval of the frequency parameters even in the presence of a strong noise. However, this does not mean that one would be able to discriminate a doublet: two different peaks separated by a small frequency compared to their own frequencies ν_1 and ν_2 (resolution). The criterion to know if we are able to discriminate two close peaks is simple: the fit L2 residual error remaining after using a two-oscillator model has to be significantly smaller than the one of a one-oscillator model. To test the performances of our methods regarding this criterion, we simulated a fictitious sample with the same parameter as in section A on which we added an oscillator at slightly higher frequency. Then, we used our methods trying to fit the data coming from this fictitious sample using first one oscillator and then two oscillators. The results depending on the separation of the two oscillators ***δν*** are shown in FIG. 6.

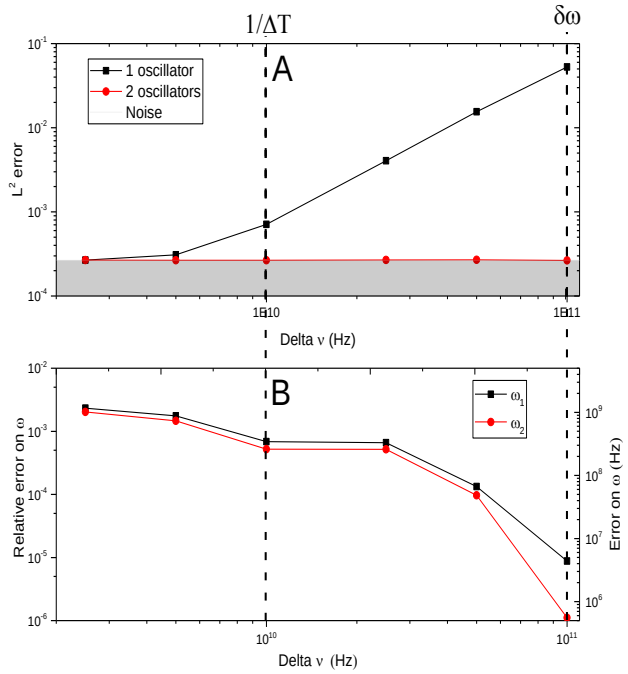

FIG. 6. A- L^2 residual error on the fit using one or two oscillators (gray area depict the limitation due to the added noise); B- relative error on the ω_1 and ω_2 parameters. Here one can see that we are not limited by the width of the resonance but by the duration of the time trace.

One can see that the resolution of our fit is clearly bellow the width, ***δω***, of the peaks themselves. However, we are limited by the temporal window of the experiments (100 ps). With the time-domain fit, a doublet will give a beat note, meaning a low frequency envelop on a high frequency carrier wave. Thus, if the signal-to-noise ratio is high enough, the only limitation will be the time window of the experiment, which should be long enough to detect the variations of the envelope. Since the peaks have a finite size, the envelope will also be damped. Consequently, it will end up by being lower than the noise. From these considerations, one can derive the following equation giving the optimal time window:

$$\begin{aligned}\Delta T_{opt} &= \frac{2\pi}{\gamma}\ln\left(\frac{\tilde{A}\gamma}{2\pi\tilde{N}\delta f}\right)\\ &= \frac{2\pi}{\gamma}\left[\ln\left(\frac{\gamma}{2\pi\delta f}\right)+ln\left(\frac{\tilde{A}}{\tilde{N}}\right)\right](\delta\varepsilon,\gamma,N)\\ &= \frac{2\pi}{\gamma}\ln\left(\frac{\tilde{A}\gamma}{2\pi\tilde{N}\delta f}\right)=\frac{2\pi}{\gamma}\left[\ln\left(\frac{\gamma}{2\pi\delta f}\right)+ln\left(\frac{\tilde{A}}{\tilde{N}}\right)\right],\end{aligned} \tag{15}$$

where $\tilde{N}$ is the noise amplitude value in the frequency domain, ***δf*** is the full frequency range, and is the depth of the considered peak in the frequency domain. It is important to note that $\tilde{A}$ and $\tilde{N}$ are power spectral densities and thus are expressed in “amplitude square per Hertz” units. Finally, it is important to note that the term ***δf*** is in fact the inverse of the time sampling rate. To summarize, as expected, the resolution of the proposed methods is higher than the width of the peak and is still is limited by the frequency resolution of the discreet Fourier Transform.

D. Validation with multiple-oscillator Drude-Lorentz model

To validate the method with a more complex sample, we simulated one fictitious sample (like a carbohydrate) made of six oscillators with parameters given in Table 1.

	Targeted value			Relative Error (%)		
#	$\Delta\varepsilon$	$\omega/2\pi$ (THz)	$\delta\gamma/2\pi$ (THz)	$\Delta\varepsilon$	$\omega/2\pi$	$\delta\gamma/2\pi$
1	10^{-3}	0.3	0.1	0.03	0.003	0.1
2	2.10^{-3}	0.5	0.01	10^{-3}	3.10^{-5}	0.004
3	10^{-2}	1	0.5	0.1	0.008	0.02
4	10^{-2}	1.1	0.55	0.1	0.01	0.05
5	0.1	2.5	0.1	0.01	0.003	0.04
6	10^{-3}	3.5	0.1	0.8	0.03	3

TABLE 1 : TARGETED VALUES FOR THE FIT AND CORRESPONDING RELATIVE ERRORS

Those parameters lead to a refractive index depicted in FIG. 7 and subsequently the spectrum (

FIG. 8).

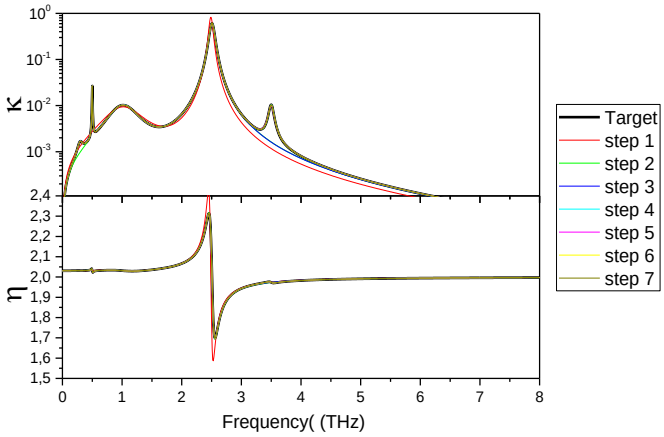

FIG. 7 Targeted refractive index versus frequency compared to the one calculated at each step of the fit (additional oscillators)

Thus, it is important to act as if we did not know any parameter of the sample but the thickness. From the spectrum, one can see several deeps (four). An additional absorption feature can be seen in the retrieved refractive index around 0.5 THz being the fifth deep. Five deeps mean 18 parameters which is enormous if one intends to directly find the result as it is (taking only 10 values for each parameter would mean a volume of 10^{18} sets of parameters to test). Consequently, we began to fit the two strongest oscillators (the one leading to the deep at a frequency a bit higher than 1 THz and the one around 2.5 THz) and then to add the next oscillators one by one to strongly diminish the volume of the space of the possibilities. The new oscillators were added by picking the one corresponding to the most important residual error in the spectrum (as seen in

FIG. 8 B) leading to a decrease of the error as shown in Table 2

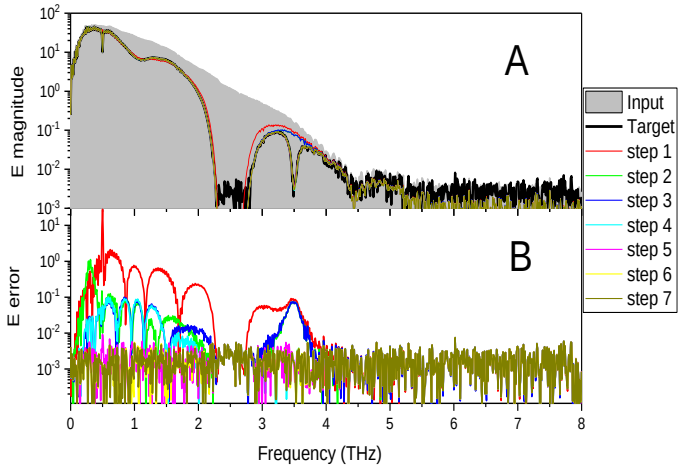

FIG. 8 A- Targeted spectrum compared to the one fitted at each step, in gray - the spectrum of the input. B – L^2 Residual error spectrum at each step.

Step #	1	2	3	4	5	6	7
Number of oscillators	2	3	4	5	6	6	6
L^2 Residual error in %	11	0.8	0.23	0.19	0.028	0.0269	0.0268

TABLE 2 : L^2 RESIDUAL ERROR DEPENDING ON THE NUMBER OF OSCILLATORS OF THE FIT

Here, one can see that the residual error decreases step by step with additional oscillators. Moreover, in

FIG. 8 B) it is clear that the addition of a new oscillator decreases the residual error in the frequency range where the oscillator is added. After the step #4, it is clear that a residual error remains in the region around 1 THz. Thus, we added a sixth oscillator that strongly decreased the residual error. Indeed, this is due to the fact that in this region two oscillators were put in the model (Table 1). Finally, because the convergence was not fully obtained, we performed the sixth and seventh steps to refine the precision by fitting in a closer space of the parameters previously obtained. This resulted in precision and resolution similar to the ones obtain in FIG. 5 for each oscillator. Indeed, the higher is the frequency of the oscillator the lower is the signal and thus the lower is the precision. These results show that the methods is not only valid for one or two oscillators but for a set including six oscillators, even if two of those oscillators are close together in frequency similarly to the example of **FIG. 6**.

To summarize the first validations on fictitious samples, we proved that Fit@TDS enables retrieving of the one-oscillator Drude-Lorentz model very accurately, even in a presence of a noise comparable to a single shot video time-frame measurement in a commercial THz-TDS system. We showed that the proposed method is capable to identify two different peaks of the two-oscillator Drude-Lorentz model with a resolution power depending on the total time span of the recording and not on the width of those peaks as far as the measurements are not noise limited. We gave a formula (eq 15) to know the optimum time span for THz-TDS measurements. Finally, we tested Fit@TDS on an example including six oscillators adopting an iterative use of the methods. The obtained results were at the same precision and resolution as for a smaller amount of oscillators only limited by the noise.

Nevertheless, it is important to test it on real samples. For instance, with such samples we always knew at an ultimate precision the set thickness of the sample as well as the other parameters. In a real case, the thickness will be measured at a relative precision and may vary on the surface of the sample. In addition, the other parameters will have to be inferred from the experiments and not from an artificial input.

V. VALIDATION WITH REAL SAMPLES

After testing the method on fictitious samples, it was used on real samples. First, on two high resistivity 5-mm-thick silicon wafers, then on a lactose pellet and finally on a metasurface made of gold split ring resonators on quartz substrate.

A. Silicon wafer sample

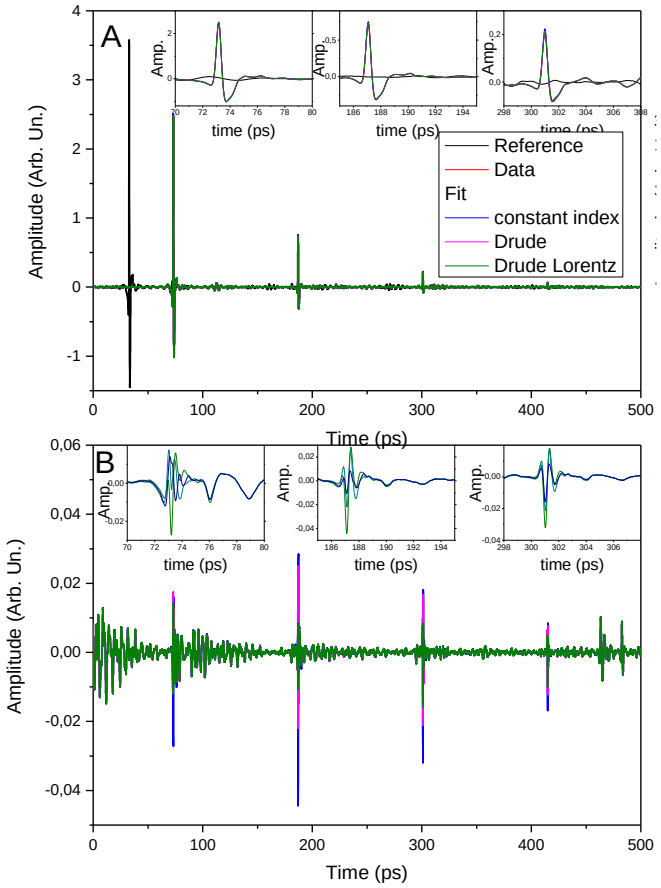

FIG. 9 A time trace of the Si wafer experiments (inset zoom on the main peak and the two first echoes), B residual error in the time domain.

A high resistivity silicon is a typical reference sample for THz-TDS, several historical studies since the beginning of THz-TDS has been published [4, 36, 16, 37], and thus is a good starting point to test the method. A float zone high resistivity (>10 kΩ.cm) silicon wafer with the thickness of 5 mm ± 1 % were purchased from Sil'tronix S T. We measured the thickness with a digital thickness comparator from Mitutoyo to be 5016±4 µm. It has to be noted that a remaining overestimation exist on this value since any imperfection on the wafer or dust between the wafer and the marble plate will induce additional thickness. We performed the THz-TDS measurement at 23± 1°c on a time range of 560 ps with a step of 33 fs. Before plotting and treating the data, we boxcar filtered them in the frequency domain below 160 GHz to remove spurious parasitic modes. The time traces and the corresponding spectra are presented respectively in FIG. 9 and 10.

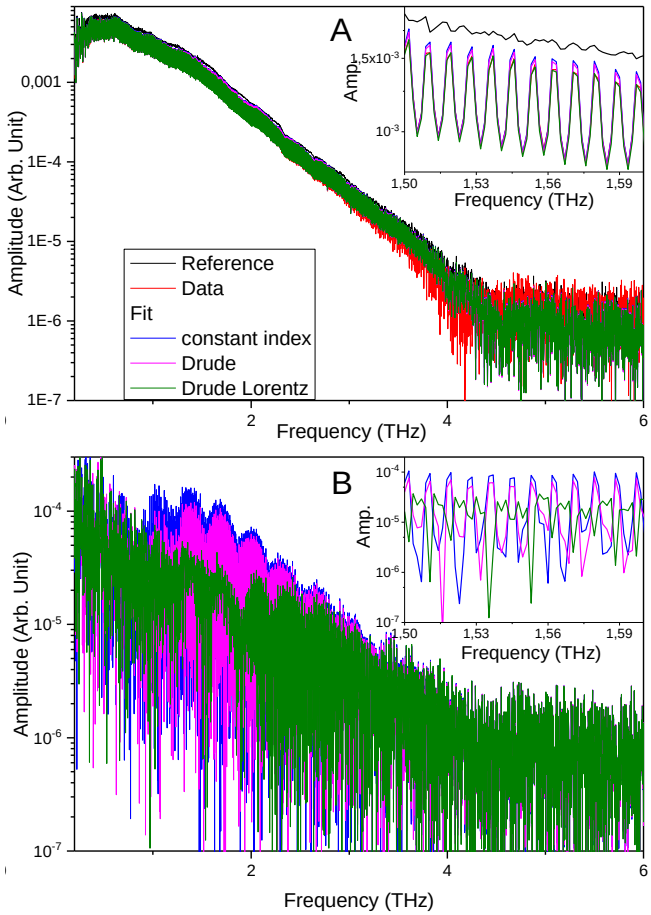

FIG. 10 A spectra corresponding to time trace of FIG 9 (inset zoom between 1.5 and 1.6 THz), B residual error in the frequency domain.

Such samples are usually modeled using the Drude model [38]. Consequently, we fitted the data using first a non-dispersive permittivity (constant index), then a pure Drude model and finally the Drude-Lorentz model with an oscillator to take into account low energy branch of phonons [39, 40]. The complex refractive indexes for all the three models are plotted in FIG. 11 and the corresponding parameters in Table 3.

Firstly, looking at FIG. 9 & 10 we can conclude that the fit worked more than fairly for all the three models and this is confirmed by the small value of residual error found in Table 3. Secondly, one can see in the time domain that the time position of the residual error is clearly physical and thus can be interpreted. The first residual error from 0 ps is an artifact due to the box car filtering and can be seen at lower magnitude close to the end of the time trace. Then the main source of residual error is perfectly time-correlated to the recorded pulses, and does not show any specific spectral feature, meaning that the models do not perfectly fit the experiments. This is the case for constant index and Drude model since one can see a real improvement by implementing the Drude-Lorentz model. For the residual error in the case of the Drude-Lorentz model, the fact that the frequency domain residual error follows fairly the index of a pulse and that an oscillation at the Fabry-Pérot period is observed in the frequency domain may indicate again that the model could be not fully satisfactory. In fact, models that are more sophisticated have already been drawn for silicon in the THz domain as the one of ref [41] based on the microscopic transport on which one can add a Lorentz oscillator to take into account the low energy phonon or impurities absorption.

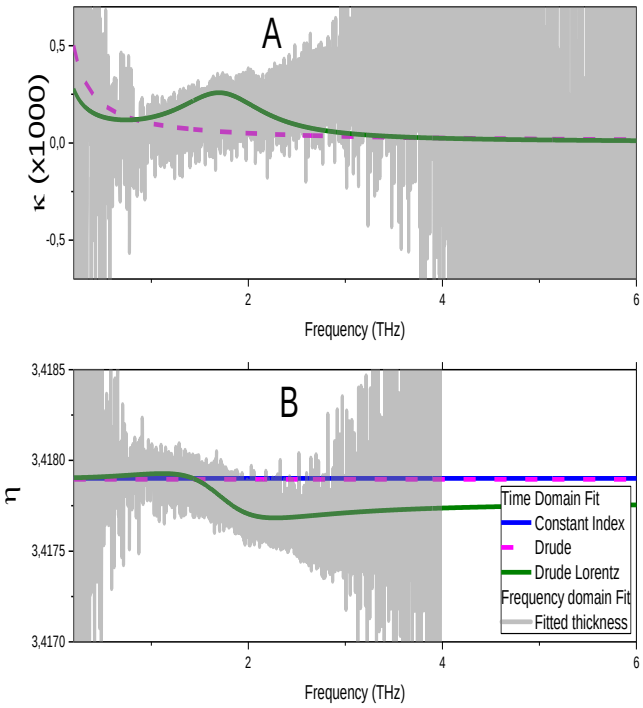

FIG. 11 fitted Refractive index of the two Si wafers modeled with no oscillator and a Drude oscillator. The frequency domain fit was done using the thickness obtained from the time domain fit.

Model	No dispersion	Drude	Drude Lorentz
Residual Error %	2.736	2.527	2.405
T (mm)	4.99908	4.99909	4.99907
ε	11.68204	11.68201	11.68113
$\omega_p/2\pi$ (THz)		4.19	18.82
$\gamma_p/2\pi$ (THz)		25 700	964 617
χ			0.00093
$\omega_0/2\pi$ (THz)			1.79
$\gamma_0/2\pi$ (THz)			1.10

TABLE 3 : PARAMETERS FOR SILICON REFRACTIVE INDEX FOR THE THREE MODELS FOUND BY THE TIME DOMAIN FIT.

To go a step further the refractive indices retrieved by time domain and frequency domain methods were plotted in FIG. 11. It has to be empathized that the thickness used for the fit in the frequency domain was the one extracted from the fit in the time domain: 4.99908 mm, which is in good agreement with the comparator measurement. Indeed, we performed as well the fit with the measured thickness but got a shit of -0.01 in the refractive index and more importantly additional noisy oscillation of amplitude ~$1.5 10^{-3}$ on the refractive index are visible showing that the measured thickness for three points on the wafer does not correspond to the average thickness on the wafer. There one can see that the time domain model is in total agreement with the frequency domain model showing first the coherence of the methods. Moreover, the method is very precise and gives the effective thickness value fully pertinent for the study.

When going to the fit parameters of the Drude-Lorentz model, firstly, we agree with the literature on the global value for refractive index [16]. Secondly, one can see that both the frequency and the width of the Lorentz oscillator end to be very close to the one reported in ref [40], showing the reliability of the method. To conclude on this part, we were able to get the refractive index and absorption of a high resistivity silicon wafer at a high precision. Considering the effect of jittering in time measurement in equation (13) as the fact that we did not measure refractive index of nitrogen gas in the band that may induce systematic error, we trust the three first digits of this refractive index. Trusting the fourth one would require additional stabilization (temperature) and measurements that is not in the scope of this paper. Still we found values very close to the metrological one in the literature with a quicker and simpler method that is more than satisfactory for most of the applications.

B. Lactose pellet

If silicon is a perfect first example, it does not have much features to be fitted in the THz THz-TDS range. Thus, we used the methods on a pellet of -lactose monohydrate (CAS 5989-81-1) powder with purity ≥ 99% total lactose basis

(determined by gas chromatography)) purchased at Sigma Aldrich. Due to the fragility of the pellet, it was extremely difficult to measure the thickness; still we measured roughly 900 µm with a ± 20-µm uncertainty. To fit the data we followed the methodology used in section IV. We first plotted (not shown) the transmission data and found two strong peaks and numerous Fabry-Pérot oscillations. Thus, we fit using the two-oscillator model. The resulting L^2 residual error shows two additional oscillators plus losses at high frequency. Consequently, we added three oscillators to take into accounts those features. The fit results are shown in FIG. 12 superimposed with frequency domain fitted refractive indexes and Table 4 shows the fit results.

Again, because the results were better than with comparator-measured thickness we took the thickness from the time domain fit to retrieve the refractive indices in the frequency domain. Frequency domain and time domain indices are in good agreement at low frequency. However, from the highest peak around 1.37 THz till the end of the spectral band, an important discrepancy exists. This is because for a strong absorption peak, the phase is lost in the frequency domain and thus the algorithm is not able to unwrap it properly [22]. This example clearly shows the robustness of the proposed methods considering this issue. To go a step further, one can see that three absorption peaks are distinguishable with corresponding feature in the real part of the refractive index. The peaks at 0.53 THz [42, 43], 1.17 THz [44, 45] and 1.37 THz [46, 47] are the characteristic absorption peaks of α-lactose monohydrate [10, 44, 48]. The peak at 1.81 THz is more difficult to measure (higher frequency and vicinity of a water line) and thus is more rare in the literature but was already reported [47] and maybe due to the presence of an anhydrous phase [49].

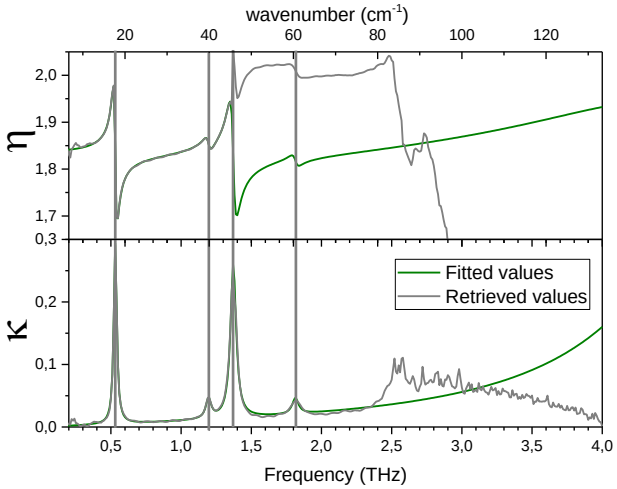

FIG. 12 Fitted value with the time domain method in green and frequency domain fit in gray. The time domain methods avoid the problem linked to the loss of the phase in the frequency domain due to a too strong absorption.

Additionally, one can see that the retrieved value for η starts to be wrong after the strongest absorption peak at 1.37 THz. Indeed, at this frequency the signal fall into the noise and thus the phase is extremely noisy leading to the mistake in the phase unwrapping. Finally, the high frequency losses shape does not match the lorentzian bell shoulder of the hypothetical strong infrared absorption. Thus, we tentatively attributed this last feature to losses due to the scattering in the pellet made of nano-crystallites powder.

#	χ	$\omega_0/2\pi$ THz / cm^{-1}	$\gamma_0/2\pi$ GHz
1	0.052351	0.5303 / 17.69	25.8
2	0.031530	1.3699 / 46.69	47.8
3	0.004434	1.1951 / 39.86	45.2
4	0.002738	1.8137 / 60.50	54.1
5	*0.509754*	*5.0764 / 169.3*	*1618*

TABLE 4 : RESULTS OF THE FIT OF THE LACTOSE PELLET WITH FIVE OSCILLATORS. THE FIFTH OSCILLATOR IS USED TO FIT SCATTERING LOSSES.

To summarize, we were able to retrieve the frequency, the width and the oscillator strength of four oscillators in the 0.2 to 2.5 THz range. Still improvement could be done by including scattering in the model as it was done in the frequency domain in [24].

C. Metamaterial on quartz

To go a step further we used Fit@TDS on an artificially structured material, a metasurface. Metasurfaces are spreading their use in the THz range, for example as narrowband terahertz modulator [50] or light matter interaction enhancers [51]. Having precise insight of the properties of such component will quicken the optimization of the fabrication process

and allow the design of better metasurfaces. Thus, we fabricated a metasurface made of the split ring resonator (200 nm of Au and 20 nm of Ti) on top of a 200 µm-thick crystalline quartz substrate (z-cut) using e-beam lithography and lift off. The SEM picture of the metasurface is shown in FIG. 13.

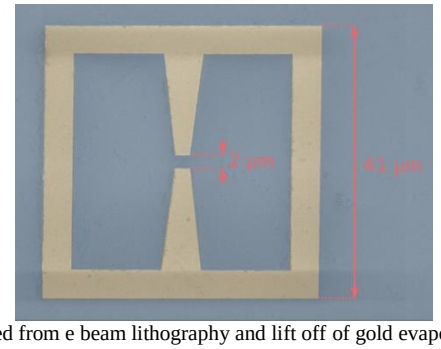

FIG. 13 SRR SEM images of the metasurface fabricated from e beam lithography and lift off of gold evaporated onto a quartz substrate.

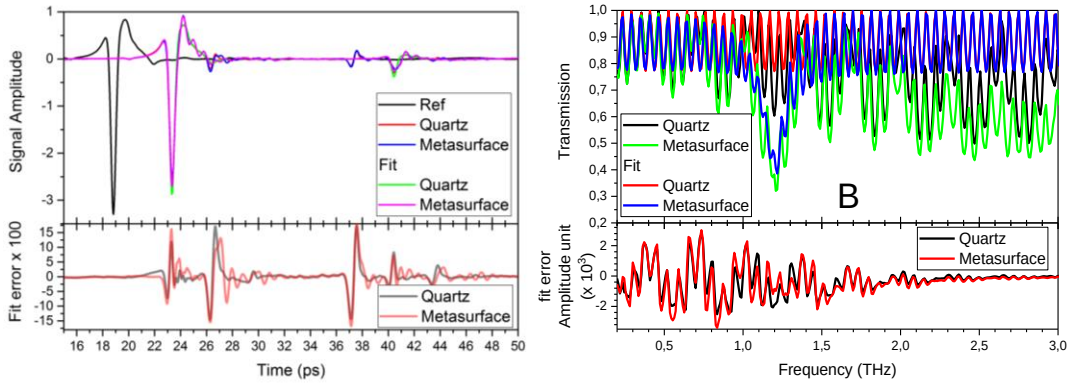

FIG. 14 A) Top - time trace of the result and the fit, bottom - the residual error; B) top - frequency domain transmission, bottom - frequency domain error (amplitude unit).

The filling factor of quartz covered by metal is ~7% corresponding to the hypothesis (see III.B for details). To perform the experiments, we tied the samples on top of a 1-mm-thick quartz substrate to prevent any interference between the near field modes of the metasurface and the back interface of the thin substrate. The samples were then measured and fitted. As a first step the thickness and refractive index of the quartz without metasurface was retrieved to compare with the one found in the fit of the metasurface. Both results are shown in FIG. 14.

There, one can see that the fit succeed with good precision (respectively 9.2% and 10.7% residual error). From the temporal residual error, we can deduce that the small residual error comes from two different reasons. First, two temporal pulses are not fitted by the model around 27 and 37 ps. Those two peaks correspond to unwanted reflections at the thick / thin quartz substrate undoubtedly due to a thin air layer between them (the peak at 27 ps corresponds to propagation through ~ 211 µm of quartz the one at 37 ps to 973 µm). This account for most of the residual error (~70%). Then, remains a residual error temporally correlated to the main peak. One cannot see any specific spectral feature of this residual error when doing the Fourier transform of this peak. We attributed this to the modification due to the previously reported effect. Indeed, since energy appears in other peaks, it has to be removed from the main one.

Still it allows the retrieval of the parameters of the metasurface as shown in Table 5.

Sample	Quartz	Metasurface
T (mm)	1.2092	1.2101
ε	4.50	4.49
ω_{meta} (THz)		1.220
Q_0		24.15
Q_{E1}		18.40
Q_{E2}		5.26
Q_{TOT}		6.11
$\delta\theta$ *(Rad.)*		0.363

TABLE 5 : PARAMETERS FOR METASURFACE TDCMT FIT. THE QUALITY FACTOR DEFINE AS $Q = \omega\tau/2\,\Delta T_{opt}$ GIVEN FOR SAKE OF USE; Q_{TOT} IS CALCULATED AS IN [31].

Firstly, the found parameters are coherent regarding the material refractive index. Secondly, Q_{tot} corresponds the one found by dividing the frequency by the width of the transmission deep. Both confirm that the method works. Then, the method allows going a step further in making the difference between external losses (75%) and absorption losses

(25%) that is close to the value usually found in simulation. Finally, since the metasurfaces are processed on a quartz/air interface, it is clearly non-symmetric. The coupling coming from the quartz is about three time higher that the coupling coming from air. This is again expected from momentum conservation law and correspond to the depths of the observed peak as demonstrated in [52].

To summarize, Fit@TDS allowed to retrieve all the parameter of a resonant mode of a metasurface showing that not only material parameter can be retrieved using the methods but also photonic parameters. In addition, the residual error of the fit was clearly related to experimental perturbation helping a researcher to understand the experiment.

VI. Conclusion

In this paper, we presented a new method, and an associated software whose code is given in the link of ref [28], to fit THz THz-TDS data with material and metamaterial model based on time domain fit. The goal of the software is to provide better and more precise insight of unknown sample as well as to quicken the process in the case of a known sample for quality control for instance. We first explained the methods, then tested it on fictitious samples and finally on real ones: a semiconductor, a molecular crystal and a metamaterial. Compared to other software's and methods Fit@TDS has five main advantages. Firstly, a precise measurement of the thickness of the sample is not needed since it plays the same role as the other fit parameters. In fact, precise measurement of the thickness of a sample such as carbohydrates but also semiconductor wafers at sub micrometer precision is challenging and avoiding this step is a real improvement. Secondly, since we take the refractive index problem as a whole and thus have only a small number of parameters compared to the usual two parameters per frequency, we are way less perturbed by the noise letting us to reach really high index precision ($< 10^{-3}$ for the silicon wafer due to the system limitation). Thirdly, since the fit residual error is in amplitude units, one can clearly make interpretation of the residual error leading to better interpretation of the experiments and possible mistake of the model used. Especially this can reveal imperfections in the experiments as on the quartz/metasurface experiments. Fourthly, since we are fitting in the time domain the phase is not lost in case of strong absorption and additional step is not needed [22] as shown with the experiments on lactose. Finally, it allows precise, reliable and consistent retrieving of material parameters using Drude-Lorentz model but as well of metamaterial with TDCMT giving access to the metal losses and external losses of the metamaterial as well as the coupling directivity.

Indeed, this method is not limited to THz-TDS systems and can be applied to any time-domain spectroscopic system as soon as one has an access to the electric or magnetic-field. For instance, implementing this method with a dual-comb spectroscopy system (for review on ASOPS see [53]) would allow the following of the fit parameters versus time at a 20 kHz rate! To further enlarge the area of application it is possible to simply change the model in the software open source code. It will be then possible to simulate other materials for instance taking into account scattering similarly to [24] or using Debye-derivated models for liquid or impregnated samples [54] or even combine it further with mixture identification methods [55]. Additionally, since it enables to simulate the photonic part, it will be possible to implement circuits made of THz resonators [56] or any THz photonics dispersive element or components [48].

Since the residual error of the parameters reach the system limitation, an improvement of the performances needs improvement of THz-TDS systems. For instance, several groups in the world are working on producing emission antenna able to deliver more powerful and broadband pulses [57] as well as better detection systems [58]. Furthermore, it will be very convenient to decrease to the minimum the post pulse emission of the antenna. This will allow the use of additional denoising technics [59] and thus improve the bandwidth and the precision of the fit.

To conclude, we hope that the community will take over Fit@TDS and implements further options corresponding to their needs. Indeed, the first step will be to implement a model more specific to their sample, but a step further could be for instance to implement a model to determine gas concentration of a known gas mix, or of doping or impurity concentration in a known material. Overall, because it works on mainstream computer and OS's, we hope that Fit@TDS will become a valuable tool for the community and will help the spreading of THz-TDS towards new fields of research.

References

[1] G. Mourou, C. V. Stancampiano, and D. Blumenthal, "Picosecond microwave pulse generation," *Applied Physics Letters*, vol. 38, no. 6, pp. 470–472, 1981. [Online]. Available: https://doi.org/10.1063/1.92407

[2] D. H. Auston, K. P. Cheung, and P. R. Smith, "Picosecond photoconducting hertzian dipoles," *Applied Physics Letters*, vol. 45, no. 3, pp. 284–286, 1984. [Online]. Available: https://doi.org/10.1063/1.95174

[3] R. Sprik, I. Duling III, C.-C. Chi, and D. Grischkowsky, "Far infrared spectroscopy with subpicosecond electrical pulses on transmission lines," *Applied physics letters*, vol. 51, no. 7, pp. 548–550, 1987.

[4] D. Grischkowsky, S. Keiding, M. Van Exter, and C. Fattinger, “Far-infrared time-domain spectroscopy with terahertz beams of dielectrics and semiconductors,” *JOSA B*, vol. 7, no. 10, pp. 2006–2015, 1990.

[5] J. F. Lampin, L. Desplanque, and F. Mollot, “Detection of picosecond electrical pulses using the intrinsic franz?keldysh effect,” *Applied Physics Letters*, vol. 78, no. 26, pp. 4103–4105, 2001. [Online]. Available: https://-doi.org/10.1063/1.1381030

[6] M. Hangyo, M. Tani, and T. Nagashima, “Terahertz time-domain spectroscopy of solids: a review,” *International journal of infrared and millimeter waves*, vol. 26, no. 12, pp. 1661–1690, 2005.

[7] D. M. Mittleman, R. Jacobsen, R. Neelamani, R. G. Baraniuk, and M. C. Nuss, “Gas sensing using terahertz time-domain spectroscopy,” *Applied Physics B: Lasers and Optics*, vol. 67, no. 3, pp. 379–390, 1998.

[8] D. Bigourd, A. Cuisset, F. Hindle, S. Matton, R. Bocquet, G. Mouret, F. Cazier, D. Dewaele, and H. Nouali, “Multiple component analysis of cigarette smoke using thz spectroscopy, comparison with standard chemical analytical methods,” *Applied Physics B*, vol. 86, no. 4, pp. 579–586, 2007.

[9] A. Markelz, S. Whitmire, J. Hillebrecht, and R. Birge, “Thz time domain spectroscopy of biomolecular conformational modes,” *Physics in Medicine and Biology*, vol. 47, no. 21, p. 3797, 2002.

[10] B. Fischer, M. Hoffmann, H. Helm, G. Modjesch, and P. U. Jepsen, “Chemical recognition in terahertz time-domain spectroscopy and imaging,” *Semiconductor Science and Technology*, vol. 20, no. 7, p. S246, 2005. [Online]. Available: http://stacks.iop.org/0268-1242/20/i=7/a=015

[11] S. Song, F. Sun, Q. Chen, and Y. Zhang, “Narrow-linewidth and high-transmission terahertz bandpass filtering by metallic gratings,” *IEEE Transactions on Terahertz Science and Technology*, vol. 5, no. 1, pp. 131–136, 2015.

[12] D.-K. Lee, G. Kim, C. Kim, Y. M. Jhon, J. H. Kim, T. Lee, J.-H. Son, and M. Seo, “Ultrasensitive detection of residual pesticides using thz near-field enhancement,” *IEEE Transactions on Terahertz Science and Technology*, vol. 6, no. 3, pp. 389–395, 2016.

[13] M. Geiser, C. Walther, G. Scalari, M. Beck, M. Fischer, L. Nevou, and J. Faist, “Strong light-matter coupling at terahertz frequencies at room temperature in electronic lc resonators,” *Applied Physics Letters*, vol. 97, no. 19, p. 191107, 2010.

[14] G. Scalari, C. Maissen, S. Cibella, R. Leoni, P. Carelli, F. Valmorra, M. Beck, and J. Faist, “Superconducting complementary metasurfaces for thz ultrastrong light-matter coupling,” *New Journal of Physics*, vol. 16, no. 3, p. 033005, 2014.

[15] J. Sun and S. Lucyszyn, “Extracting complex dielectric properties from reflection-transmission mode spectroscopy,” *IEEE Access*, vol. 6, pp. 8302–8321, 2018.

[16] L. Duvillaret, F. Garet, and J.-L. Coutaz, “A reliable method for extraction of material parameters in terahertz time-domain spectroscopy,” *IEEE Journal of selected topics in quantum electronics*, vol. 2, no. 3, pp. 739–746, 1996.

[17] ——, “Noise analysis in thz time-domain spectroscopy and accuracy enhancement of optical constant determination,” in *Optoelectronics’ 99-Integrated Optoelectronic Devices*. International Society for Optics and Photonics, 1999, pp. 38–48.

[18] O. S. Ahmed, M. A. Swillam, M. H. Bakr, and X. Li, “Efficient optimization approach for accurate parameter extraction with terahertz time-domain spectroscopy,” *J. Lightwave Technol.*, vol. 28, no. 11, pp. 1685–1692, Jun 2010. [Online]. Available: http://jlt.osa.org/abstract.cfm?URI=jlt-28-11-1685

[19] J. C. Lagarias, J. A. Reeds, M. H. Wright, and P. E. Wright, “Convergence properties of the nelder–mead simplex method in low dimensions,” *SIAM Journal on optimization*, vol. 9, no. 1, pp. 112–147, 1998.

[20] W. C. Davidon, “Variable metric method for minimization,” *SIAM Journal on Optimization*, vol. 1, no. 1, pp. 1–17, 1991.

[21] J.-F. Bonnans, J. C. Gilbert, C. Lemaréchal, and C. A. Sagastizábal, *Numerical optimization: theoretical and practical aspects*. Springer Science & Business Media, 2006.

[22] M. Bernier, F. Garet, J. L. Coutaz, H. Minamide, and A. Sato, “Accurate characterization of resonant samples in the terahertz regime through a technique combining time-domain spectroscopy and kramers-kronig analysis,” *IEEE Transactions on Terahertz Science and Technology*, vol. 6, no. 3, pp. 442–450, May 2016.

[23] I. Pupeza, R. Wilk, and M. Koch, “Highly accurate optical material parameter determination with thz time-domain spectroscopy,” *Opt. Express*, vol. 15, no. 7, pp. 4335–4350, Apr 2007. [Online]. Available: http://-www.opticsexpress.org/abstract.cfm?URI=oe-15-7-4335

[24] Z. Li, Z. Zhang, X. Zhao, H. Su, H. Zhang, and J. Lan, “Linewidth extraction from the thz absorption spectra using a modified lorentz model,” *Journal of Infrared, Millimeter, and Terahertz Waves*, vol. 34, no. 10, pp. 617–626, Oct 2013. [Online]. Available: https://doi.org/10.1007/s10762-013-0007-2

[25] T. D. Dorney, R. G. Baraniuk, and D. M. Mittleman, “Material parameter estimation with terahertz time-domain spectroscopy,” *JOSA A*, vol. 18, no. 7, pp. 1562–1571, 2001.

[26] O. S. Ahmed, M. A. Swillam, M. H. Bakr, and X. Li, “Efficient material parameters estimation with terahertz time-domain spectroscopy,” in *Terahertz Technology and Applications IV*, vol. 7938. International Society for Optics and Photonics, 2011, p. 793805.

[27] W. Zhu, C. Li, G. Zhang, and G. Fang, “The calculation of dielectric dispersive models in thz range with ga,” *Microwave and Optical Technology Letters*, vol. 49, no. 10, pp. 2540–2545, 2007.

[28] R. Peretti. (2018) fit@tds github repository. [Online]. Available: https://github.com/THzbiophotonics/Fit-TDS

[29] R. E. Perez, P. W. Jansen, and J. R. R. A. Martins, “pyOpt: A Python-based object-oriented framework for nonlinear constrained optimization,” *Structures and Multidisciplinary Optimization*, vol. 45, no. 1, pp. 101–118, 2012.

[30] P. Jansen and R. Perez, “Constrained structural design optimization via a parallel augmented lagrangian particle swarm optimization approach,” *Computers & Structures*, vol. 89, no. 13, pp. 1352 – 1366, 2011. [Online]. Available: http://www.sciencedirect.com/science/article/pii/S0045794911000824

[31] C. Manolatou, M. Khan, S. Fan, P. Villeneuve, H. Haus, and J. Joannopoulos, “Coupling of modes analysis of resonant channel add-drop filters,” *Quantum Electronics, IEEE Journal of*, vol. 35, no. 9, pp. 1322–1331, 1999.

[32] R. Peretti, G. Gomard, C. Seassal, X. Letartre, and E. Drouard, “Modal approach for tailoring the absorption in a photonic crystal membrane,” *Journal of Applied Physics*, vol. 111, no. 12, p. 123114, 2012. [Online]. Available: http://-link.aip.org/link/?JAP/111/123114/1

[33] Y. Shi and R. C. Eberhart, “Empirical study of particle swarm optimization,” in *Evolutionary computation, 1999. CEC 99. Proceedings of the 1999 congress on*, vol. 3. IEEE, 1999, pp. 1945–1950.

[34] P. J. Angeline, “Using selection to improve particle swarm optimization,” in Evolutionary Computation Proceedings, 1998. IEEE World Congress on Computational Intelligence., The 1998 IEEE International Conference on. IEEE, 1998, pp. 84–89.

[35] “http://www.menlosystems.com/en/products/thz-time-domain-solutions/terasmart-terahertz-spectrometer/.” [Online]. Available: http://www.menlosystems.com/en/products/thz-time-domain-solutions/terasmart-terahertz-spectrometer/

[36] M. Van Exter and D. Grischkowsky, “Carrier dynamics of electrons and holes in moderately doped silicon,” *Physical Review B*, vol. 41, no. 17, p. 12140, 1990.

[37] S. Nashima, O. Morikawa, K. Takata, and M. Hangyo, “Measurement of optical properties of highly doped silicon by terahertz time domain reflection spectroscopy,” *Applied physics letters*, vol. 79, no. 24, pp. 3923–3925, 2001.

[38] T. Ohba and S. Ikawa, “Far?infrared absorption of silicon crystals,” *Journal of Applied Physics*, vol. 64, no. 8, pp. 4141–4143, 1988. [Online]. Available: https://doi.org/10.1063/1.341325

[39] A. Abdullah, K. Maslin, and T. Parker, “Observation of two-phonon difference bands in the fir transmission spectrum of si,” *Infrared Physics*, vol. 24, no. 2, pp. 185 – 188, 1984. [Online]. Available: http://www.sciencedirect.com/-science/article/pii/002008918490068X

[40] J. Dai, J. Zhang, W. Zhang, and D. Grischkowsky, “Terahertz time-domain spectroscopy characterization of the far-infrared absorption and index of refraction of high-resistivity, float-zone silicon,” *J. Opt. Soc. Am. B*, vol. 21, no. 7, pp. 1379–1386, Jul 2004. [Online]. Available: http://josab.osa.org/abstract.cfm?URI=josab-21-7-1379

[41] K. J. Willis, S. C. Hagness, and I. Knezevic, “A generalized drude model for doped silicon at terahertz frequencies derived from microscopic transport simulation,” *Applied Physics Letters*, vol. 102, no. 12, p. 122113, 2013. [Online]. Available: https://doi.org/10.1063/1.4798658

[42] M. Walther, M. R. Freeman, and F. A. Hegmann, “Metal-wire terahertz time-domain spectroscopy,” *Applied Physics Letters*, vol. 87, no. 26, p. 261107, 2005. [Online]. Available: https://doi.org/10.1063/1.2158025

[43] D. Allis, A. Fedor, T. Korter, J. Bjarnason, and E. Brown, “Assignment of the lowest-lying thz absorption signatures in biotin and lactose monohydrate by solid-state density functional theory,” *Chemical Physics Letters*, vol. 440, no. 4, pp. 203 – 209, 2007. [Online]. Available: http://www.sciencedirect.com/science/article/pii/S0009261407004794

[44] W. Withayachumnankul, B. M. Fischer, and D. Abbott, “Material thickness optimization for transmission-mode terahertz time-domain spectroscopy,” *Opt. Express*, vol. 16, no. 10, pp. 7382–7396, May 2008. [Online]. Available: http://www.opticsexpress.org/abstract.cfm?URI=oe-16-10-7382

[45] B. B. Jin, Z. X. Chen, Z. Li, J. L. Ma, R. Fu, C. H. Zhang, J. Chen, and P. H. Wu, in *34th International Conference on Infrared, Millimeter, and Terahertz Waves*, Sept 2009, pp. 1–2.

[46] J. A. Zeitler, K. Kogermann, J. Rantanen, T. Rades, P. F. Taday, M. Pepper, J. Aaltonen, and C. J. Strachan, “Drug hydrate systems and dehydration processes studied by terahertz pulsed spectroscopy,” *International journal of pharmaceutics*, vol. 334, no. 1, pp. 78–84, 2007.

[47] Y. Kawada, T. Yasuda, A. Nakanishi, K. Akiyama, and H. Takahashi, “Single-shot terahertz spectroscopy using pulse-front tilting of an ultra-short probe pulse,” *Opt. Express*, vol. 19, no. 12, pp. 11228–11235, Jun 2011. [Online]. Available: http://www.opticsexpress.org/abstract.cfm?URI=oe-19-12-11228

[48] R. Peretti, F. Braud, E. Peytavit, E. Dubois, and J.-F. Lampin, “Broadband terahertz light–matter interaction enhancement for precise spectroscopy of thin films and micro-samples,” *MDPI photoncics*, vol. 5, no. 2, p. 11, 2018.

[49] G. Smith, A. Hussain, N. I. Bukhari, and I. Ermolina, “Quantification of residual crystallinity of ball-milled, commercially available, anhydrous β-lactose by differential scanning calorimetry and terahertz spectroscopy,” *Journal of Thermal Analysis and Calorimetry*, vol. 121, no. 1, pp. 327–333, Jul 2015. [Online]. Available: https://doi.org/-10.1007/s10973-015-4469-4

[50] T. A. P. Tran and P. H. Bolivar, “Terahertz modulator based on vertically coupled fano metamaterial,” *IEEE Transactions on Terahertz Science and Technology*, pp. 1–1, 2018.

[51] B. Qin, Z. Li, F. Hu, C. Hu, T. Chen, H. Zhang, and Y. Zhao, “Highly sensitive detection of carbendazim by using terahertz time-domain spectroscopy combined with metamaterial,” *IEEE Transactions on Terahertz Science and Technology*, vol. 8, no. 2, pp. 149–154, March 2018.

[52] G. Gomard, R. Peretti, E. Drouard, X. Meng, and C. Seassal, “Photonic crystals and optical mode engineering for thin film photovoltaics,” *Opt. Express*, vol. 21, no. S3, pp. A515–A527, May 2013. [Online]. Available: http://-www.opticsexpress.org/abstract.cfm?URI=oe-21-103-A515

[53] T. Ideguchi, A. Poisson, G. Guelachvili, N. Picqué, and T. W. Hänsch, “Adaptive real-time dual-comb spectroscopy,” *Nature communications*, vol. 5, p. 3375, 2014.

[54] M. Lazebnik, M. Okoniewski, J. H. Booske, and S. C. Hagness, “Highly accurate debye models for normal and malignant breast tissue dielectric properties at microwave frequencies,” *IEEE Microwave and Wireless Components Letters*, vol. 17, no. 12, pp. 822–824, 2007.

[55] Y. Peng, C. Shi, M. Xu, T. Kou, and Y. Zhu, “Qualitative and quantitative identification of components in mixture by terahertz spectroscopy,” *IEEE Transactions on Terahertz Science and Technology*, pp. 1–1, 2018.

[56] D. W. Vogt and R. Leonhardt, “Ultra-high q terahertz whispering-gallery modes in a silicon resonator,” *APL Photonics*, vol. 3, no. 5, p. 051702, 2018. [Online]. Available: https://doi.org/10.1063/1.5010364

[57] M. Fang, K. Niu, Z. Huang, W. E. I. Sha, X. Wu, T. Koschny, and C. M. Soukoulis, “Investigation of broadband terahertz generation from metasurface,” *Opt. Express*, vol. 26, no. 11, pp. 14241–14250, May 2018. [Online]. Available: http://www.opticsexpress.org/abstract.cfm?URI=oe-26-11-14241

[58] O. Kliebisch, D. C. Heinecke, and T. Dekorsy, “Ultrafast time-domain spectroscopy system using 10 ghz asynchronous optical sampling with 100 khz scan rate,” *Opt. Express*, vol. 24, no. 26, pp. 29930–29940, Dec 2016. [Online]. Available: http://www.opticsexpress.org/abstract.cfm?URI=oe-24-26-29930

[59] J. Dong, A. Locquet, M. Melis, and D. Citrin, “Global mapping of stratigraphy of an old-master painting using sparsity-based terahertz reflectometry,” *Scientific reports*, vol. 7, no. 1, p. 15098, 2017.